Assessment of bioenergy plant locations using a GIS-MCDA approach based on spatio-temporal stability maps of agricultural and livestock byproducts: A case study

Zhan Shi [a], Francesco Marinello [a], Ping Ai [b], Andrea Pezzuolo [a,c,*]

[a] Department of Land, Environment, Agriculture and Forestry, University of Padova, Legnaro, PD 35020, Italy
[b] College of Engineering, Huazhong Agricultural University, Wuhan 430070, China
[c] Department of Agronomy, Food, Natural Resources, Animals and Environment, University of Padova, Legnaro, PD 35020, Italy

HIGHLIGHTS

- Farm byproducts were explored for bioenergy to achieve SDGs and carbon neutrality.
- GIS-MCDA was combined with machine learning to assess impacts on bioenergy potential.
- Spatiotemporal and DEMATEL bridge the biosphere–anthroposphere nexus for bioenergy.
- For stable 10^{12} kJ biogas from rice/wheat biomass, the MCDA pinpointed 45–66 sites.
- A scalable bioenergy model is presented, which can boost sustainability and guide policies.

GRAPHICAL ABSTRACT
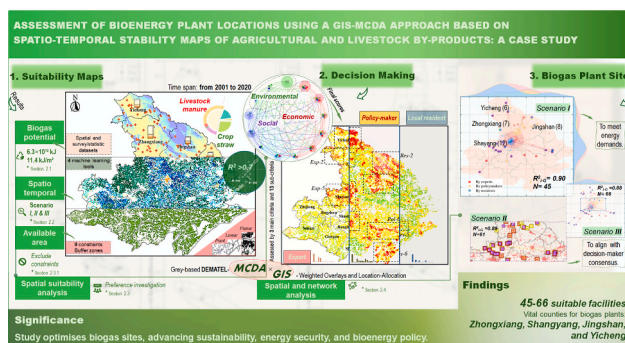
ARTICLE INFO

Editor: Jacopo Bacenetti

ABSTRACT

Addressing the global challenge of energy sustainability and global directives on farming emissions, the United Nations, the European Union, and China have led with strict targets for clean energy, renewable share growth, and carbon neutrality, highlighting a commitment to collective sustainability. This work is situated within the ambit of the Sustainable Development Goals (SDGs), advocating for a transition towards renewable energy sources. With substantial and accessible bioenergy resources, notably in Hubei Province, China, biogas technology has emerged as an emission-cutting solution. This research, focused on the Jianghan Plain, employs an integrated approach combining spatial analyses with machine learning tools to evaluate crop yield stability over two decades, with the aim of maximising the biogas yield from agricultural byproducts, i.e., crop straw and livestock manure. Using Multi-Criteria Decision Analysis (MCDA), which is informed by grey-based DEMATEL, 9 constraints and 13 environmental, social, and economic criteria were assessed to identify optimal sites for biogas facilities. The findings underscore the significant bioenergy potential of agricultural byproducts from the plain of 6.3×10^{12} kJ/year at an 11.4 kJ/m^2 density. Stability analyses revealed consistent biomass availability, with rice in Gongan and Shayang and wheat in Jiangling being the primary contributors. Through the MCDA, 45–66 optimal biogas plants were identified across 4 critical counties (Zhongxiang, Shangyang, Jingshan, and Yichen),

balancing the energy supply and demand under various stable scenarios. Furthermore, this study demonstrated the criticality of moderate biomass stability for stakeholder consensus and identified areas of high stability essential for energy demand fulfilment. Theoretically, this study offers a practical model for bioenergy resource exploitation that aligns with global sustainability and carbon neutrality goals to address the urgent need for renewable energy solutions amidst the global energy crisis. Practically, this study sets a precedent for policy and planning in environmental, agricultural, and renewable sectors, signifying a step forwards in achieving environmental sustainability and an energy-efficient future.

1. Introduction

The global energy landscape is facing a significant crisis, primarily due to an overreliance on non-renewable energy sources and the environmental impacts associated with their use. This situation necessitates a shift towards renewable energy sources, aligning with the 2030 Agenda for Sustainable Development (SDGs) (Willett et al., 2019). In response, the United Nations (UN) aims for global clean energy access by 2030 and net zero emissions by 2050, and has secured over $400 billion for clean energy initiatives (UNDP, 2021). Simultaneously, the European Union (EU) updated its Renewable Energy Directive, setting ambitious goals for member states to reach a 32 % renewable energy share by 2030, which was later raised to 40 % (EU, 2021). China is working towards achieving carbon neutrality by 2060, aiming to reduce its greenhouse gas (GHG) emissions by 2.3 billion tonnes, prioritising a transition towards renewable energy and reducing its reliance on coal (IEA, 2021).

Agricultural byproducts are considerable and accessible for bioenergy production. In Europe, the annual potential of these bioresources is estimated at 950 million tonnes (Kumar Sharma et al., 2022), while it was estimated at 4 billion tonnes globally in 2018, primarily consisting of 20 % crop straw and 70 % livestock manure (Zhao et al., 2018). Fully utilising agricultural byproducts can significantly address the energy crisis and environmental pollution, promoting renewable energy (SDG 7) and sustainable land use (SDG 15) (Adamu et al., 2023). To this end, policies and guidelines have been enacted to facilitate bioenergy production from farm and biomass handling, reducing its environmental impacts (2001/81/EC, 2001). Biogas technology offers a promising solution (Liang et al., 2023a, 2023b). For instance, the EU has experienced significant growth in biogas electricity, with an installed capacity of 11.9 GW, generating 55.8 TWh (Eurostat, 2020). Moreover, the capacity of biogas to reduce GHG emissions by 115 t with just 10,000 m^3 underscores its crucial role in China's efforts to achieve carbon neutrality by 2060 (Li, 2022). Specifically, Hubei Province in central China, which generates 10 % of the total agricultural byproducts, is an ideal site for biogas development due to the high energy demand coupled with the current energy shortage (Liu et al., 2023). With its extensive agriculture and high crop straw and livestock manure production, the Jianghan Plain in Hubei provides a strong foundation for biogas technology.

However, evaluating the wide-ranging impacts, including the technical, environmental, social, and economic advantages, of biogas projects is crucial for aiding bioenergy planning on the plain (Ferrari et al., 2022b). To sustainably leverage the bioenergy potential of agricultural byproducts, advanced modelling techniques capable of handling nonlinear agricultural data patterns are essential. Among artificial intelligence (AI) methods, the backpropagation neural network (BP-ANN) stands out for its effectiveness in deciphering nonlinear relationships in datasets influenced by dynamic climate changes (Shi et al., 2023). It has demonstrated remarkable accuracy in predicting crop yields and bioenergy potentials (Elavarasan, 2020). For bioenergy potential estimation, Shi et al. (2024) used BP-ANN to demonstrate that crop straw had a potential of 2.1×10^9 MJ on the Jianghan Plain of Hubei ($R^2 > 0.83$). They utilised the accumulated net primary productivity (NPP, kgC/m^2) of crops as it prioritises crop distribution more effectively. For livestock manure, Liu et al. (2023) demonstrated that the biogas potential of plains from livestock manure was 9×10^8 MJ, which is 28.28 % lower

than that from straw. As CSY (2022) reported, the annual biogas production in this plain is $>4 \times 10^8$ MJ via large-scale biogas projects (AD volume > 500 m^3).

To fully harness bioenergy potential, thorough spatial analysis is vital for optimising bioresource exploitation and simplifying the supply chain, given the dispersed nature of agricultural byproducts such as crop-sown areas (Yan et al., 2021). Thus, creating stable crop spatiotemporal maps is crucial for accurately calculating straw yield to assess biogas production feasibility and efficiency, as shown in previous multitemporal yield pattern analyses (Blasch et al., 2020). The innovation of combining multiple yield maps has been demonstrated using PCA and K-Means clustering to reveal long-term variability and stability. This approach identifies consistent high-yield zones that affect straw availability (Pascucci et al., 2018). In addition to PCA and K-means, tools such as hierarchical clustering, quantile-based binning, and decision trees are used to delineate stability zones through statistical learning and pattern recognition, benefiting from the "no free lunch" principle (Table S4) (Shi et al., 2023). Integration of algorithms can enhance large dataset clustering for efficiency, scalability, and flexibility and can also minimise errors (Sarker, 2022). Moreover, apart from the integration of both crop grain yield and pasture total green dry matter to form a Stability Index (McEntee et al., 2020), the spatiotemporal presence of crops can also be utilised by assessing the frequency and regularity of crop appearances rather than only the yield amounts. This approach allows for effective mapping of biomass availability for energy production and is critical for ensuring a reliable biomass supply for biogas production.

Guided by biogas potential estimates and spatiotemporal stability maps, the strategic development of biogas plants aims to achieve efficient allocation. A key strategy involves siting plants near settlements for district heating use, offsetting hosting drawbacks with heating advantages (Leduc et al., 2010). Alternatively, selecting sites away from densely populated areas addresses concerns related to "Not-In-My-Back-Yard" effects (Batel et al., 2013). Therefore, the criteria and constraints should be defined. Ferrari et al. (2022a) summarised three main criteria, i.e., social, economic, and environmental. They defined 8 constraints, e.g., water bodies, road networks, and harvesting costs, for multicriteria decision models/analyses (MCDM/A) (Hajkowicz and Collins, 2007). Among these methods, the analytic hierarchy process (AHP), despite being used the most often (58 %), has limitations in modelling, such as consistency and non-interpretability (Saaty, 1987). To address this issue, the fuzzy decision-making trial and evaluation laboratory (F-DEMATEL) method, which is used in 5 % of reviewed MCDM/A articles due to complex data processing, effectively structures criteria and scores, especially with the grey sharpening process (Bai and Sarkis, 2013). This approach navigates the subjectivity and uncertainty in decision-making when gathering survey data and offers insight into criteria interrelationships at biogas plant sites (Jeong and Ramírez-Gómez, 2018). Technically, the geographic information system-multicriteria decision analysis (GIS-MCDA) method for spatial assessment can be used to optimise site selection and supply-demand schemes. GIS-MCDA integrates spatial data with multicriteria decision-making processes, allowing for comprehensive evaluation of various factors in geographic contexts (Brahma et al., 2016). Ferrari et al. (2021b) demonstrated the significance of land use and efficiency in biogas plant development, with further research emphasising its effectiveness in distributing supply hubs for community benefits across localities, where spatial/network
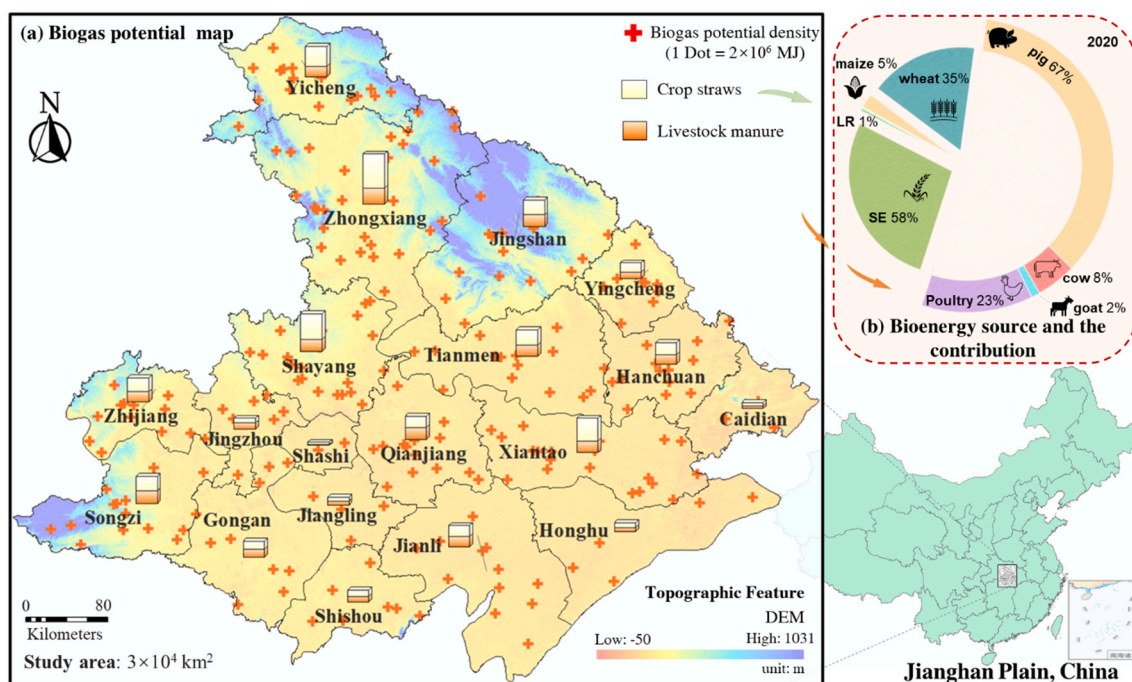
Fig. 1. Topographic map of the study area: (a) biogas potential map and (b) bioenergy sources and contributions. Biogas potential from crop straw and livestock manure are marked with crosses. The stacked bars in (a) show storage potential and proportions, and the point density indicates the distribution. The pie chart in (b) shows the 2020 bioenergy sources from four types of straw and manure, with nearly equal contributions. SE-rice straw and pig manure were the largest contributors. The data are from Table 1.

analysts are widely used (Jesus et al., 2021).

Previous studies have focused mainly on crop residues such as straw, but our work uniquely integrates both straw and livestock manure, considering crop variability and the latest field research. This holistic approach improves biogas potential assessments and enhances practical applications in diverse agricultural settings. By including policy impacts and ensuring data interpretability, our study contributes to more informed and effective bioenergy policies. Therefore, our study aims to answer the following questions:

- What is the distribution of biogas potential from straw and livestock manure on the Jianghan Plain in relation to crop spatiotemporal stability?
- What outcomes do biogas plants yield, considering diverse viewpoints, and what dynamics govern the decision-making elements?
- Where are the optimal biogas plant sites, and how well do they balance supply and demand under differing stakeholder perspectives and spatiotemporal conditions?

Leveraging GIS-MCDA, our research provides innovative insights into optimal biogas plant siting, offering a scalable solution for renewable energy and carbon neutrality. This approach advances bioenergy technology, promotes sustainable practices, and minimises environmental impacts. Our findings can impact bioenergy policy, potentially setting new standards in environmental, agricultural, and renewable energy domains and advancing a sustainable, energy-efficient future.

2. Materials and methods

2.1. Data preparation and collection

2.1.1. Study area

The Jianghan Plain in Hubei, a leading agricultural region, is particularly well suited for bioenergy research and plant siting due to its supportive policies, advantageous geography, and favourable agro-

climate (Shi et al., 2024). This study investigated 19 counties, as shown in Fig. 1(a).

Crop straw (8×10^9 kg, 91 % of annual production, i.e., from rice, wheat, and maize) and livestock manure (2×10^{11} kg, 96 %, i.e., from pigs, cows, goats, and poultry) are key biomass sources (CSY, 2022). Rice is typically categorised as single-season early rice (SE-rice) or late double-season rice (LR-rice) based on its phenological traits and cultivation methods.

2.1.2. Data collection

This research primarily used spatial and survey/statistical datasets encompassing 8 types of data: crop maps, crop primary productivity, geographic and socioeconomic spatial elements, site suitability questionnaires, cost surveys, and livestock production (e.g., number of livestock, feeding cycles, and production-discharge coefficients) (Ferrari et al., 2021a). Table 1 lists the data sources, and descriptions are presented in Table S1.

The spatial data included the ChinaCropPhen, TerraClimate, MOD17A3HGF, and point of interest (POI) databases, along with administrative regions and road network systems. Some data, such as crop primary productivity for calculating biogas potential from straw, were based on previous findings (Shi et al., 2024). Data analysis was conducted by GIS, involving functions such as spatial analysis (e.g., reclassification, resampling, masking, zonal statistics), and optimisation using network analysis (e.g., location-allocation), ensuring consistency in the temporal-spatial dimensions and resolution. Specifically, all the data were resampled to a 1 km resolution (~1 km) for spatial analysis.

The survey/statistical datasets were essential for calculating biogas yield and siting biogas plants, and are shown in Table 2 (biomass-to-energy conversion coefficients) and Table S2. For site suitability, we distributed questionnaires to global surveyors (Section 2.3) using MCDA to analyse 20 valid responses and generate overlay weights for spatial analysis (Section 2.4).

The datasets are described in Table S1.

Table 1
Breakdown and description of data collection.

Spatial database	Data sources	Geospatial type/ counts	Period	Data extraction	Unit	Details
Crop maps	ChinaCropPhen (Luo et al., 2020)	Raster (~1 km resolution)	2001–2019	Crop planting areas	km²	For SE-rice, late LR-rice, maize, wheat
	ChinaCP (Qiu et al., 2022)	Raster (~500 m)	2015–2020			
Net primary production (NPP)	(Shi et al., 2024)	Raster (~500 m)	2001–2020	Accumulated NPP	kgC	
	MOD17A3hgf (Running and Zhao, 2021)	Raster (~500 m)	2001–2020	NPP/GPP	kgC	
GIS datasets (Table 3)	NASADEMhgt (Zeng et al., 2023)	Raster (~30m_DEM)	2000	Slope degree (SL)	degree	–
	LandScan_HD (Lloyd et al., 2019)	Raster (~90 m)	2022	Population density (PD)	km⁻²	–
	GDPGrid_China (Huang et al., 2014)	Raster (~1 km)	2010	GDP per capita (GDP)		–
	China Historical Geographic Information System (CHGIS) (Dong et al., 2017)	Vector (polylines/ points:13)	2013	Gas pipelines (GP)	km	Gas pipelines and nodes
	OpenStreetMap (OSM) (Zhao et al., 2021)	Vector (polylines:37,660)	2019	Road network density (RN)	km	Railways, expressways (max speed: 110 km/h), national roads (80), provincial roads (80), city roads (60)
		Vector (polylines:1243)		Water bodies (WB)	km	Rivers, canals
		Vector (polygon:959)			km²	Lakes, pools
		Vector (polygon:8349)		Residential & accommodation (RA)		Building layouts
Points of Interest Map (POIs)	Amap and Baidu-Map (Zeng et al., 2023)	Vector (points:17,075)	2022	RA	–	Houses, apartments, hotels, resorts
		Vector (points:1645)		Scenic area (SA)		Historic/scenic spots, natural reservations
		Vector (points:57,746)		Public services (PS)		Cultural services, bureaus, health care facilities
		Vector (points:187,154)		Commercial & shopping (CS)		Financial centres, shopping malls
		Vector (points:31,241)		Corporate & industrial (CI)		Industrial zones, agriculture/forestry areas

Statistic database	Data acquisition	Geographic scope	Period	Data extraction	Unit	Details
Site suitability survey	AHP questionnaires	Global (20 surveyors, 13 constraints, 9 levels)	2023	MCDA final scores (Table 4)		Suitability criteria and levels (1–9)
Comprehensive use of agricultural byproducts	Field survey (Ferrari et al., 2022b; Liu et al., 2023), Yearly books (statistical records) (CSY, 2022)	County level	2021	Harvesting costs (HC)	CNY	Transport costs, packing costs
				Transport radius	km	Cut-off values (radius < 30 km)
				Livestock manure production	kg	Yearly production of pigs, cattle, goats and poultry, daily production of manure, and feeding days of livestock
				Biomass seasonality (BS)	kg	Storage capacity, biomass stability scenarios (I-III)
				Straw utilisation	–	Off-field straw use for fuel, feed, base, fertiliser, and materials (Table S2)
			2001–2020	Facility data		Facility upgrades and efficient-use rates
Biogas projects	Yearly books	City level[a]	2019	Large-scale projects (AD volume > 5000 m³)	m³	Existing projects (108), biogas production (1.8×10^7 m³) (Table 5)

[a] City: Refers to a prefecture-level city in China overseeing multiple counties. County: An administrative division under city governance, including urban and rural areas.

2.1.3. Biogas potential and analysis

The biogas potential/density calculations are based on data listed in Tables 2 and S2. The data are from Table 1 (CSY, 2022) and Liu et al. (2023). For calculations, based on the off-field rates and facility survey (Table S2), 'Daily products' and 'Feeding days' represent the daily manure output and feeding duration before slaughter, respectively, affecting biomass estimates. 'Dry biomass' refers to demoisturised biomass, which reduces handling costs. The 'AD rate' is used to assess the anaerobic digestion efficiency for energy output, and the 'energy content' measures the energy per unit of dry biomass for biogas calculations. Moreover, the accumulated NPP values were determined in previous work using the BP-ANN model (Shi et al., 2023, 2024).

The biomass content, i.e., the accumulated NPP (straw: 8.4×10^9 kg) and manure production averaged 6.3×10^9 kgC and 1.9×10^{11} kg, respectively, from 2001 to 2020. In 2020, they were 6×10^9 kgC and 1.3×10^{11} kg. This resulted in an average energy content of 6.3×10^{12} kJ, which decreased to 6×10^{12} kJ in 2020. After conversion (Table 2), the available biogas potential was 4.7×10^{11} kJ. Regional biogas density indices (BD, kJ/m²) were mapped and are displayed as density dots in Fig. 1(a), revealing a level of 11.4 kJ/m² on the plain over two decades.

2.2. Spatio-temporal stability analysis

Four crop datasets obtained from ChinaCropPhen (~1 km, 2001-2019) and ChinaCP (~500 m, 2015–2021) served as the foundational data for this work (Table 1). After ensuring consistency between the two datasets ($R^2 > 0.77$, illustrated in Fig. S1), they were merged by resampling (~1 km), masking, and reclassifying. This reclassification

Table 2
Coefficients of the biomass-to-energy conversion.

	SE-rice	LR-rice	Maize	Wheat		Pig	Cow	Goat	Poultry	Ref.
Accumulated NPP (kgC)	BP-ANN output (Shi et al., 2024).				**Daily products** (kg)	5.3	20.6	2.4	0.1	(Chiumenti et al., 2019; Ferrari et al., 2021a; Yan et al., 2021; Zhang et al., 2012)
					Feeding days	199	365	365	210	
Dry biomass	25 %				**Dry biomass**	30 %	27 %	49 %	48 %	
AD rate	0.55	0.58	0.6	0.57	**AD rate**	0.42	0.3	0.49	0.3	
Energy content (MJ/kg)	15	16	18	17	**Energy content** (MJ/kg)	21	20	12	15	

accurately labelled crop areas as "SE" (for SE-rice), "LR" (LR-rice), "Maize", and "Wheat" by phenology. Pixels that consistently represented the full phenological cycles of these four crops, described in Table S1, which combine the key stages, e.g., green-up, emergence, transplanting, heading, and maturity dates, were selected. Pixels meeting these criteria were assigned "1" for cultivated areas and "0" for non-cultivated areas.

The spatial distribution captures crop occurrences over the last 20 years, reflecting the average crop presence per county. A lower standard deviation (SD) indicates greater crop stability, which is essential for a consistent biomass supply for biogas production. This analysis involves (i) compiling 'Zonal Statistics' results (Table S3), with rows for counties and columns for statistics; (ii) identifying zones with stable (low SD) and unstable (high SD) crop occurrences, which is critical for reliable biomass availability; and (iii) pinpointing counties with high or low crop presence to inform strategic biogas plant siting.

Temporal dynamics refer to the number of pixel points in each county that have consistently appeared above a specific threshold over two decades. Here, the "threshold" delineates the frequency of crop pixel appearances, categorising the stability into high (Scenario I), medium (Scenario II), and low (Scenario III) groups. This classification, which is pivotal for agricultural management, employed clustering tools, e.g., K-Means, HC, and QB, the DT classifier, and the Jenk Natural Break algorithm (with GIS) to robustly analyse crop consistency (Table S4). The setting of clusters and thresholds highlights areas of stable/unstable crop growth, aiding in strategic planning by visualising crop occurrence stability and thus enhancing the accessibility of biomass sources in the decision-making process. According to Sarker (2022), the steps include the following:

(i) *Database call*. The analysis used 'sklearn.cluster' for K-means clustering optimisation with inertia and elbow graph visualisation. The HC employed 'scipy.cluster.hierarchy' for dendrogram creation and 'AgglomerativeClustering' for analysis. The QB used 'pandas' for weight calculations and data binning. The DT applied 'sklearn.tree' for classification by mean square error (MSE), tuning with 'max_leaf_nodes'.

(ii) *Cluster number determination*. Using the Algorithms K-Means and QB with the elbow method, HC with Ward's distances and DT with MSE and max-leaf nodes revealed the optimal number of clusters.

(iii) *Sequential clustering*. The results were grouped into optimal clusters sequentially. Stability levels were then determined by combining manual adjustments (i.e., JNB) with algorithmic analysis for accurate stability categorisation.

(iv) *Comparison and integration*. The least stable group identified by each algorithm was discarded, and the remaining data were categorised into low- to high-stability groups. These groups were then averaged across the outcomes of all algorithms to ensure a consistent and comprehensive analysis of the stability scenarios (I-III).

Furthermore, to ensure the reliability of both spatial and temporal stability, it is essential to maintain consistency by examining the correlation coefficient (R^2) between the mean values and SD from both temporal dynamic and spatial distribution analyses. A high correlation ($R^2 > 0.7$) demonstrated the consistency and variability of spatiotemporal stability for interpreting both temporal and spatial properties.

2.3. MCDA for biogas plant suitability assessment

2.3.1. Available areas

Primarily, decision-making should define theoretically available biogas plant location areas. These areas were obtained by applying a series of territorial constraints and directly removing the constraint areas (Table 3). Our study defined 9 shape-format constraints and used 'proximity' tools to create protective buffer zones (Section 3.2). Compliance with all constraints was mandatory, as failing even one results in site exclusion.

2.3.2. Preference criteria

Before the preference investigation, three main criteria were considered, namely, environmental, social, and economic aspects (Ferrari et al., 2022a), which were divided into 13 sub-criteria (Table 3). The environmental criteria included considerations such as proximity to water bodies (e.g., rivers and canals), slope gradient, and the presence of historic or scenic areas. Social criteria included population density, residential and accommodation areas, public services (e.g., cultural buildings, health-care facilities), and commercial/shopping areas (e.g., financial districts, shopping malls, supermarkets). The economic criteria included road network density, gas pipelines, corporate and industrial areas, harvesting costs (i.e., transport and packing expenses), GDP per capita, and biomass seasonality (i.e., the stability of crop planting and storage capacity in hubs).

To obtain a multidimensional assessment, participatory approaches have been included either through information based on the perception of the value of criteria or by providing the ranks/weights on the relative importance of each element. Hence, the questionnaires rated criteria from unimportant (1) to extremely important (9), with self-comparisons of 0, to assess preferences similar to the AHP method (Fig. S7(a)). The survey included 20 experts, policy-makers, and local residents who were active in rural construction and agricultural energy and who were seeking professional insights. This process yielded twenty 16×16 original matrices.

2.3.3. Grey-based DEMATEL

The grey-based DEMATEL method combines grey system theory to handle uncertainty and incomplete information, enhancing the ability of the DEMATEL method to model complex cause–effect relationships among criteria. Grey interval matrices were constructed to evaluate the assessment via the steps in Fig. S7 (Bai and Sarkis, 2013):

(i) *Upper (O_{max}) and lower (O_{min}) direct impact matrices after standardisation*. The original matrices were decomposed into lower and upper bounds to reflect the judgement range (Table S5). The lower bounds gave little importance to extreme values, reducing

Table 3
Constraints and criteria considered in biogas plant candidate sites.

Site suitability survey		Constraints		
Criteria	Subcriteria	MCDA assessment	Buffer (m)	Description
Environmental	Water bodies (WB)	Maximise distance	150 (river/canal), 300 (lake/pool)	Areas are excluded if they are too close to sensitive zones, had steep slopes (>15 %), or under 2 ha, too small for a facility.
	Slope (SL)	Minimise the slope degree	15°	
	Scenic area (SA)	Maximise distance	500	
Social	Population density (PD)	Minimise the number residing within 2 km	–	
	Residential and accommodation (RA)	Maximise distance	1000	
	Public services (PS)		300 (cultural services), 500 (bureaus), 1000 (health-care)	
	Commercial and shopping centres (CS)		300 (financial, shopping), 500 (catering)	
Economic	Road network density (RN)	Maximise road density and minimise the distance	100 (railway), 60 (expressway, national-way), 40 (provincial-way, city road)	
	Gas pipelines (GP)	Minimise distance	10	
	Corporate& industrial (CI)	Maximise distance to avoid mutual interference	100	
	Harvesting costs (HC)	Minimise harvesting costs	–	
	GDP	Maximise plants with lower GDP	–	
	Biomass seasonality (BS)	Maximise plants in high-capacity areas	–	

their impact, and adjusted middle values based on their closeness to a low point, calculated via $[1/8 + (v_{ij}\text{-}2)] \times 0.75/7$. On the other hand, the upper bounds focused on the highest values, lessening the importance of those further away via $[1/8 + (u_{ij}\text{-}1)] \times 0.75/7$, thereby thoroughly reflecting the opinions. Then, to average all the standardised metrics, O_{max} and O_{min} were obtained.

(ii) *Sharpening and Normalising Matrices (O_{sharp} and N)*. To enhance the interrelationships, we integrated the grey relational relationships to calculate O_{sharp} (Table S6):

$$s_{ij} = y_{ij} \left[Max(u_j) - Min(v_j) \right] + Min(v_j);$$

since $Min(u_j) = Min(v_j) = 0$, it was simplified to

$$s_{ij} = \frac{v_{ij} Max(u_j) - v_{ij}^2 + u_{ij}^2}{Max(u_j) - v_{ij} + u_{ij}} \quad (1)$$

where u_{ij}, v_{ij}, and s_{ij} represent the elements of Row i and Column j ($i,j = 1,2, \ldots,16$) in O_{max}, O_{min}, and O_{sharp}; we define

$$\widetilde{u}_{ij} = \frac{u_{ij} - Min(u_j)}{Max(u_j) - Min(v_j)}, \widetilde{v}_{ij} = \frac{v_{ij} - Min(v_j)}{Max(u_j) - Min(v_j)} \text{ thus}$$

$$y_{ij} = \frac{\widetilde{v}_{ij} \left(1 - \widetilde{v}_{ij} \right) + \widetilde{u}_{ij}^2}{1 - \widetilde{v}_{ij} + \widetilde{u}_{ij}}.$$

Next, to ensure comparability of the data, the chords of the two maxima were taken for normalisation of the sharpened matrices to obtain N_{max}, N_{min}, and N_{sharp} (Table S7).

(iii) *Total Relation Matrix (T) and DCMR analysis.* T was derived from N to depict the comprehensive influence among subcriteria (Table S8) since all values of N converge to a null matrix (ϑ) (Banks et al., 1997):

$$T = \left(t_{ij}\right)_{16 \times 16} = \sum_{k=1}^{\infty} N^k \xrightarrow{\vartheta = \lim_{k \to \infty} N^k} T = N(I - N)^{-1} \quad (2)$$

where I is the identity matrix.

After defining the degree of influence (D), degree of being influenced (C), degree of centrality (M), and degree of causality (R), the *DCMR* table was denoted as follows:

$$\left\{ D_i | C_i | M_i | R_i \right\} \overset{\text{def}}{=} \left\{ \sum_{j=1}^{16} t_{ji} \left| \sum_{j=1}^{16} t_{ij} \right| \sum_{j=1}^{16} \left(t_{ji} + t_{ij} \right) | \sum_{j=1}^{16} \left(t_{ji} - t_{ij} \right) \right\} \quad (3)$$

T_{max}, T_{min}, and T_{sharp} were obtained by following Eqs. (2) and (3) to construct DCMRs among the lower, sharpened, and upper matrices (Table S9), and further analysis through topological invariance underscored the significance and influence of these parameters within the decision-making network.

Subcriteria with high M, as the key nodes in the causal network, reflected both highly influencing ('influencer') and being influenced ('influencee'). Sub-criteria with positive R were denoted as the driving forces (Jeong and Ramírez-Gómez, 2018).

2.3.4. Final scores of the MCDA

We used M to determine the initial scores and R to adjust the scores for the causal network. This approach helped manifest the priorities, especially for sub-criteria of close M values, considering the influence chains (Bai and Sarkis, 2013). The process normalised M and R (as M_N and R_N), adjusted for the influence direction, and calculated the final scores (Tables 4 andS10):

$$W_i = M_{Ni} + R_{Ni} \cdot \mathscr{H}(R_{Ni}) \quad (4)$$

where $\mathscr{H}(\cdot)$ is the Heaviside step function.

Eq. (4) prioritises the influence of subcriteria on others, de-emphasising the more influenced ones. Thus, the final weights (ω_i) were calculated by W_{iN} to determine the suitability related to all criteria judged by all surveyors.

2.4. Spatial and network analysis

The dataset has 13 sub-criteria in shape, raster, and table formats, including 9 distance-related constraints (WB, SL, SA, RA, PS, CS, RN, GP, and CI, in Section 2.3.1) and 4 gradient variables (PD, GDP, HC, and BS), as outlined in Table 3. The constraints set biogas plant proximity to locations at 9 levels according to the Euclidean distance. Gradient variables guide area selection based on value preferences, classifying both data types and county-level results (BS and HC) into 9 levels by characteristics. All the data were converted to an ~30 m resolution raster format for precise analysis.

Table 4

MCDA scores for biogas plants.

Criteria		Final MCDA score (W)		
		Experts	Policy-makers	Residents
Environmental	WB	0.1880	0.1981	0.1978
	SL	0.0532	0.0335	0.0605
	SA	0.0529	0.0360	0.0979
Social	PD	0.1236	0.1043	0.0651
	RA	0.1186	0.0735	0.0847
	PS	0.0599	0.0648	0.0561
	CS	0.0575	0.0658	0.0562
Economic	RN	0.0566	0.0601	0.0592
	HC	0.0571	0.1053	0.0853
	GDP	0.0575	0.0787	0.0594
	BS	0.0574	0.0592	0.0593
	GP	0.0584	0.0601	0.0592
	CI	0.0592	0.0605	0.0593
Column sparklines (WB-CI)		▮▭▯▭▭▭▭▭▭	▮▭▯▭▭▭▭▭▭	▮▭▭▭▭▭▭▭▭

2.4.1. Spatial suitability analysis

The sensitivity analysis for biogas site selection focused on the MCDA, excluding the BD or spatiotemporal stability. Using 'weighted overlays', two sets of suitability maps were created based on three criteria (environmental, social, economic) and stakeholder views (experts, policy-makers, locals), scoring suitability from low to high (levels 1–9) through raster calculations.

Subsequently, we combined the BD and spatiotemporal stability with the MCDA, which was weighted at 25 % across the three scenarios, yielding 9 suitability maps for biogas sites. These data were then converted to shape format (points), considering land-use covers and proximity requirements for plant locations. This approach robustly identified candidates, setting solid groundwork for subsequent allocation analysis.

2.4.2. Biogas plant siting network analysis

The 'Location-Allocation' tool, part of the Network Analyst extension in ArcGIS Pro, was used for network analysis to identify the optimal sites for biogas plants from the candidate locations. This tool is used to determine the most efficient layout of facilities based on the distribution of demand points (Ferrari et al., 2022b). It helps place facilities to maximise service coverage, minimise transportation costs, and balance demand. The key inputs include:

(i) *Road networks.* This involves the geometric and technical details of the transport network, including maximum speed, one-way streets, and restricted roads (Table 3). For our analysis, the road network data were configured and input to accurately represent the actual transport routes for effective logistics planning.

(ii) *Demand points.* These are locations that require biogas services. Each point is assigned a weight indicating its significance. In our study, demand points were identified using local biomass data and consumer locations, with residential and accommodation (RA) points chosen due to their high biogas demand (Teng et al., 2022).

(iii) *Facilities.* These include 'candidates' (potential sites for biogas plants), 'required' (mandatory sites), and 'competitors' (alternative sites). Our focus was on 'candidate' sites (Section 2.4.1) to model a coordinated, noncompeting system of biogas facilities.

Additionally, the steps and parameters in our analysis include specifying a cut-off value for the maximum transport distance to model transportation costs. We applied 'Maximise Attendance' to prioritise the placement of facilities in a way that maximises the coverage of demand points.

3. Results and discussion

3.1. Spatio-temporal stability maps

Crop distribution highlights both spatial and temporal variation. Fig. 2(a) shows the spatial distribution of the four crops every five years. SE-rice and wheat dominated crop planting, with consistent distributions across counties. Fig. 2(b) shows the mean crop recurrence over time with error bars for the standard deviation (SD), indicating the frequency of the four crops in each county. More crop occurrences are illustrated in Figs. S2 and S3 to show the mean values and variability. SE-rice showed a stable, high mean and low SD, notably in Gongan and Shayang; wheat was most stable in Jiangling, followed by Zhongxiang.

For the temporal dynamics, using four algorithms, the optimal number of clusters was determined to be k = 4. This was confirmed by the elbow method, Ward's distance, and MSE analysis with max-leaf nodes (Fig. S4). SE-rice and wheat were classified as 'highly stable' for >17 occurrences, with LR-rice and maize thresholds of 11 and 5, respectively (Figs. 3(a) and S5). Excluding the least stable scenario, three stability scenarios (I-III) are depicted in Fig. 3(b). The 'Spatial Analyst'-reclassified pixel points from '2' (III) to '4' (I) for the stability of the four crops are shown in Fig. 5 and specified in Fig. S6. Additionally, it displays crop coverage stability at ~1 km resolution, with colours and shades indicating the crop types and stability. Stable and numerous SE-rice crops dominate the west, while wheat is central. In scenarios I-III, highly stable crops accounted for 24 % of the points analysed.

Moreover, Fig. 4 shows $R^2 > 0.77$ for the means and 0.86 for the SDs, indicating a strong correlation between the spatial and temporal stability, thus validating the spatiotemporal plots. These data, combined with the biogas potential (Fig. 1(a)), guided site selection via network analysis for straw logistics.

### 3.2. Available areas for siting biogas plants

The nine constraints, categorised into point, linear, and planar types, are based on the GIS layers (Fig. S11). The point data included six types across 294,867 locations: SA (1645), RA (houses, 17,075), PS (57,746), CS (187,154), GP (nodes, 6), and CI (31,241). The linear data consisted of two types over 38,917 locations: WB (river/canal, 1243), RN (37,660), and GP (pipelines, 7), with the RN including 19 railways, 2471 expressways, 1525 national ways, 4539 provincial ways, and 29,106 suburban/urban roads. The two types of planar data comprised 9308 locations: WB (lake/pool, 959) and RA (building layout, 8349) plus county-level HC and BS data derived from table-based data. Then, all constraints were overlaid with buffer zones. After applying buffer zones and additional restrictions on the GDP, SL, and PD, as specified in Table 3, a raster calculation excluding these zones identified available areas for biogas plants, as illustrated in Fig. 6.

### 3.3. MCDA determination of suitable sites for biogas plants

3.3.1. Insights on preferences and impacts

The T_{min}, T_{sharp}, and T_{max} matrices, representing the *DCMR* decision from the grey-based DEMATEL, are depicted in heatmaps (experts in Fig. 7(a), others in Fig. S12). The process, illustrated in Tables S5–S8, resulted from Eqs. (1) and (2). The lower-sharpened-upper links are depicted as the trajectories in Fig. 7(b)(c). These heatmaps clarify the general emphasis on subcriteria, revealing the diverse perspectives in decision-making. Specifically, experts preferred environmental criteria, as evident from the pronounced colour intensity, with SL and SA demonstrating a strong interrelationship indicated by their proximity in hierarchical clustering (Euclidean distance). Policy-makers preferred social criteria (PS, CS, and RA), with PS and CS being closely related. Local residents also emphasised environmental criteria.

To clarify the factors influencing decisions, Eq. (3) breaks down *T* into *DCMR* decision (Table S9) insights into the causal networks
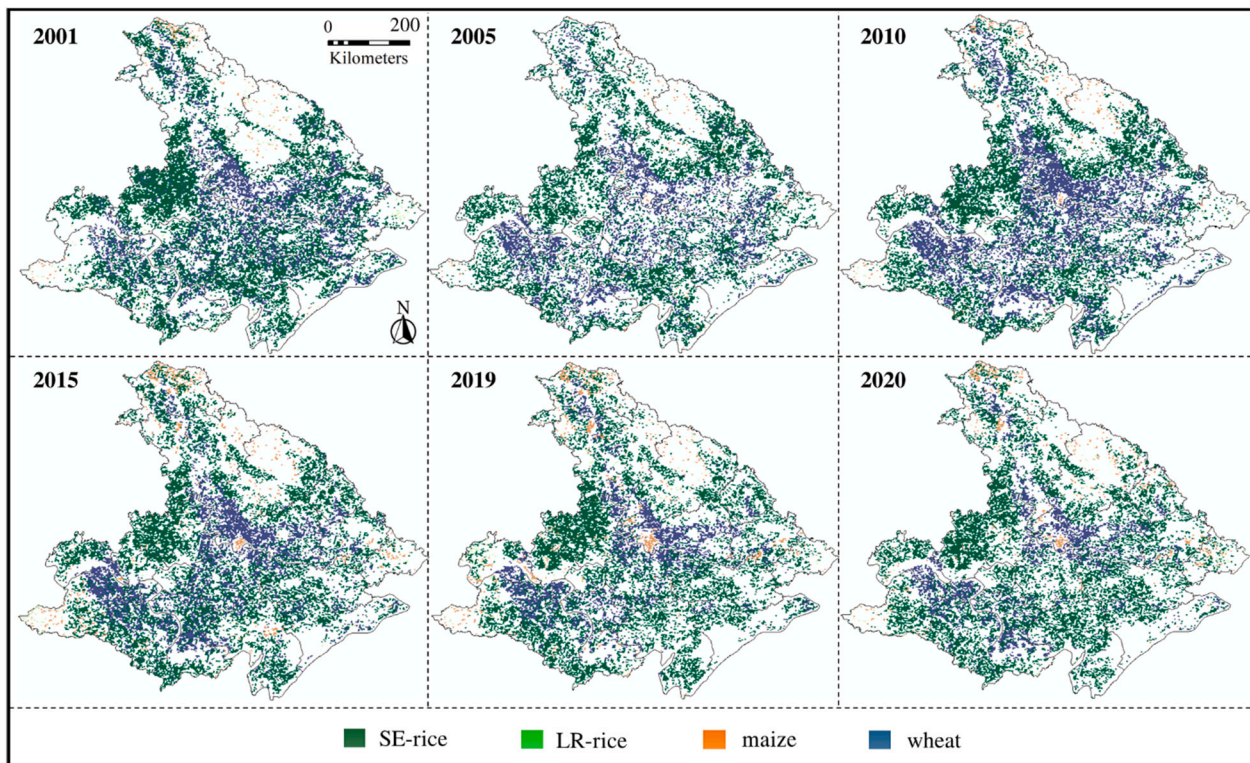
(a)
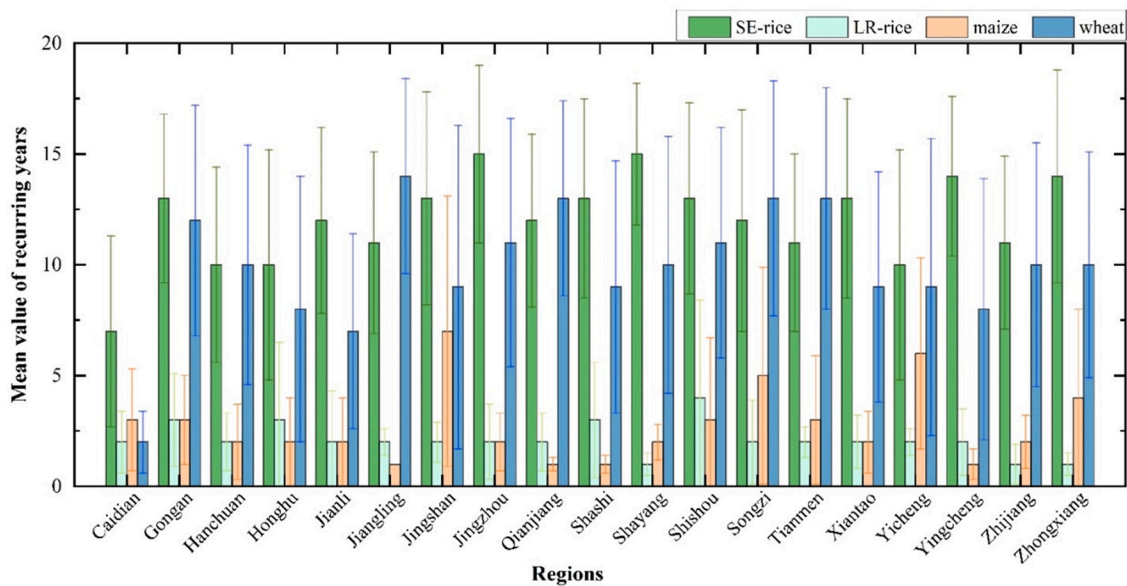
(b)

Fig. 2. Spatial distribution: (a) annual crop distribution maps and (b) county-level spatial variability statistics. The extent of cultivation of various crops remained relatively constant, with some yearly variations in number and area. The statistical significance (mean ± SD, $n = 19$) shows spatial stability across counties.

depicted in Figs. 7(d) and S12(g)(h):

(i) *Driving force.* The "centrality-causality" plots reveal the varying importance of the driving factors (subcriteria with $R > 0$) among the stakeholders. The experts focused on WB, PD, and RA (Fig. 7 (b)); the policy-makers focused on WB, HC, PD, GDP, and RA (Fig. S12(c)); and the residents focused on environmental criteria and RA, HC, and PD (Fig. S12(d)). Experts view these factors as less critical, noting most subcriteria as "the resulting ones". However, instability in these forces is suggested by overlapping

or intersecting pairs (e.g., PD × RA, CS × HC for experts; HC × PD, GDP × RA for policy-makers; RA × HC, PS × BS for residents), suggesting the potential for change with different judgements. Evidently, experts' views seem more stable, with fewer intersecting pairs. Despite varying emphases, the *M* values show slight differences across groups, underscoring the complex interplay of social and economic factors.

(ii) *Influencer* vs. *"influencee".* In the "influencing-influenced" scatterplots (Figs. 7(c), S12(e)(f)), the analysis revealed the top influencers according to the experts (WB, PD, RA, PS), policy-
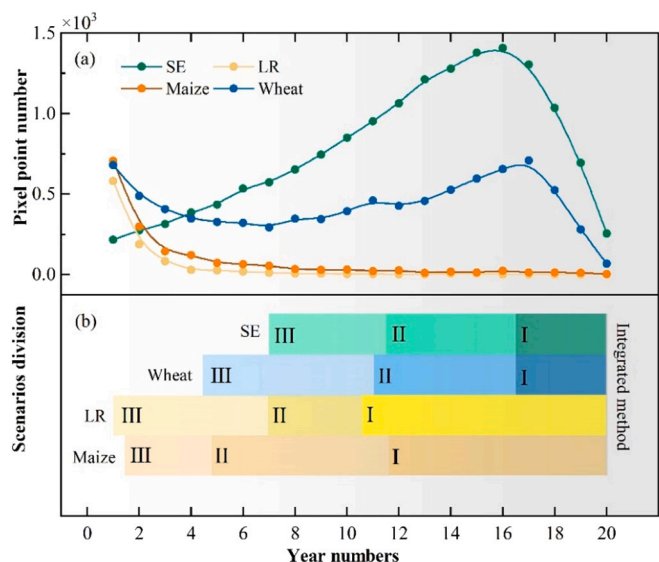
Fig. 3. Temporary dynamic analysis: (a) yearly changes in planted pixel points, (b) classification. The classification (Section 2.2), using four algorithms for temporal stability, is illustrated in Fig. S4.

makers (PD, HC, RA, WB), and residents (WB, HC, RA, PD), with WB, PD, RA, and HC emerging as key influencers. Considering environmental, social, and economic impacts, these factors should be tightly regulated. Conversely, for influencees, experts highlighted CI, GP, GDP, and CS; policy-makers chose CS, CI, PS, and GP; and residents opted for CI, CS, GDP, and BS, making CI, CS, GP, and GDP the key influencees requiring protection, especially in economic and social contexts during biogas plant construction. Additionally, it also suggests a rotation in influencers among environmental, social, and economic criteria, with environmental influencees consistently ranking last. This indicates a lesser direct impact of environmental factors on biogas plant development than their indirect effects on social and economic benefits, which are more susceptible.

(iii) *Causal networks.* An in-depth analysis of Figs. 7(d) and S12(g)–(h) revealed a diverse hierarchy of factors influencing biogas project site selection. WB stands out as a universally key environmental factor. PD and RA are also emphasised, highlighting the considerable social influence on and impacts of biogas initiatives. The

detailed significance of biogas projects was further explored by expanding on these insights (Liang et al., 2023a, 2023b).

Overall, integration of the judgement of *M* and *R* factors is essential for effectively assessing biogas plant site selection, highlighting the critical interplay between environmental, social, and economic factors.

3.3.2. Final scores of the MCDA

According to Eq. (4), the final scores (*W*) of the MCDA are presented in Tables 4 and S10. The results of a weighted overlay analysis with the final MCDA scores are depicted in Fig. S13. Among the environmental criteria, protection of water bodies and systems (WB, 56–74 %) was the most important, followed by protection of scenic and historic areas (SA, 14–27 %). Among the social criteria, the most considered criteria were the distances from the high population potential (PD, 25–34 %) and the urban or residential accommodation areas (RA, 24–33 %). Finally, among the economic criteria, the harvesting cost of straw (HC, 17–25 %) was most considered, followed by the stimulus potential for GDP growth (GDP, 16–19 %), the ability of firms to cooperate or hedge against competitive risks (CI, 14–17 %), and transport costs and accessibility (RN, BS, GP, 14–16 %).

3.4. Spatial suitability for siting biogas plants

By applying the final scores combined with the crop stability maps (Figs. 5 and S14), suitability maps based on three criteria and from three types of stakeholders were produced. The boxes showing 'Env', 'Soc', and 'Eco' in Fig. 8 and 'Exp', 'Pol', and 'Res' in Fig. S15 indicate the most suitable areas, providing a strategic balance of conditions conducive to biogas development.

For environmental protection, the top biogas project sites, i.e., 'Env-1' in western Yicheng, 'Env-2' in northern Jingshan, and 'Env-3' in central-western Shayang, were identified. These sites had 299 pixels at the highest environmental suitability (level 9 in Fig. 8(d)), with a substantial presence at levels 7 and 8. They were also prominent in social and economic evaluations. Socially, the highly suitable areas are evenly spread, enhancing community living but excluding central Tianmen, western Zhijiang and Jingzhou, and eastern Caidian, with 13,557 pixels at level 9. Economically, the 604 pixels at level 9 for top suitability are focused in the northern, central, eastern, and southeastern areas across nine counties, e.g., Yicheng and Zhongxiang, favouring plains near logistic routes and avoiding northeastern slopes (Fig. 1(a)). This reflects a strategy to minimise costs and boost economies in populous yet less
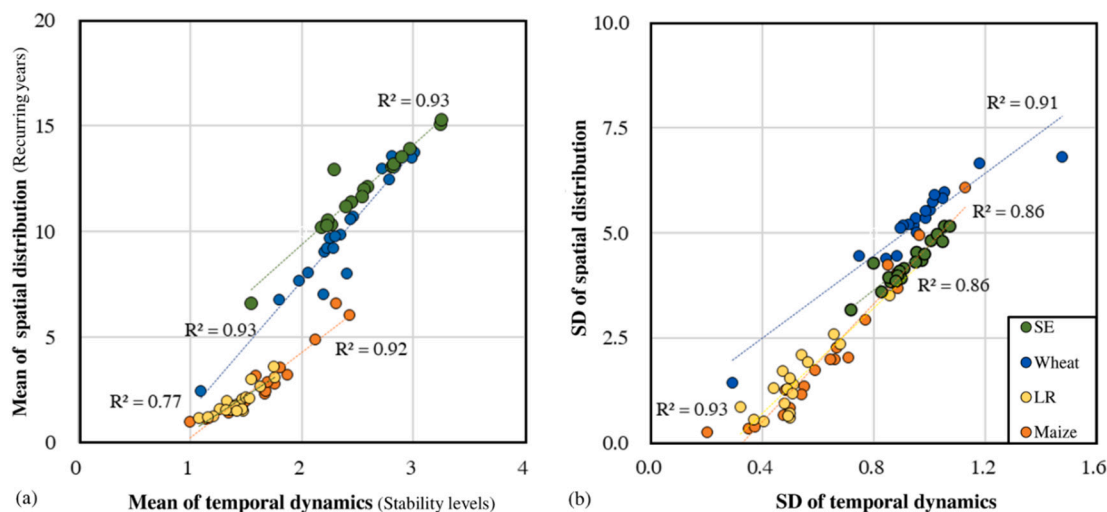

Fig. 4. Spatio-temporal consistency tests using (a) mean values and (b) SD. The R^2 value, calculated using the SST and SSE via R^2 = 1 − SSE / SST, indicates a strong correlation and consistency in the spatial distribution and temporal dynamics.
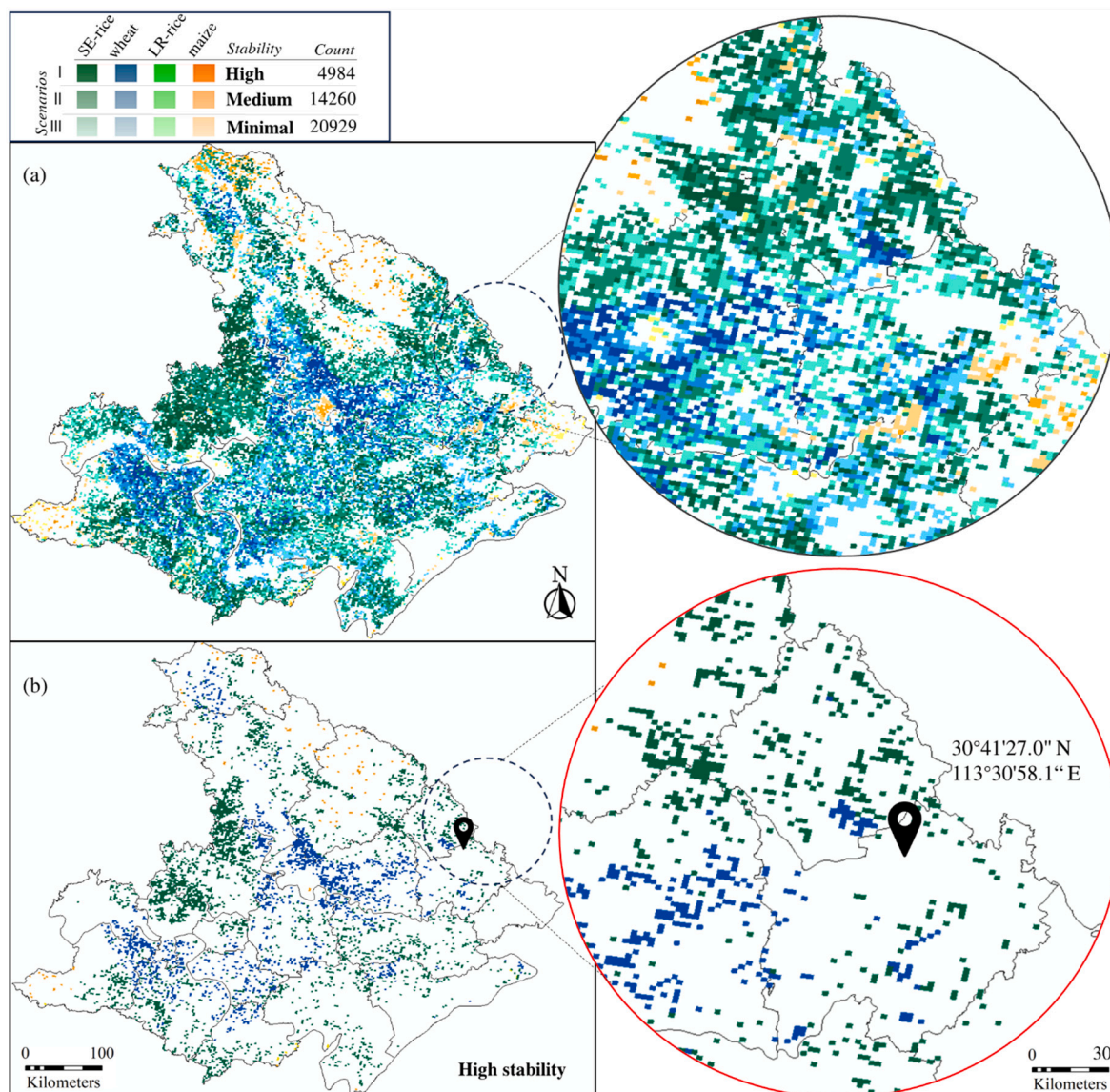
Fig. 5. Crop stability maps: (a) three scenarios fused with local magnification and (b) a high-stability scenario.

affluent regions, with social criteria showing broader high suitability coverage than economic criteria, which prioritises strategic locations (Dreher et al., 2024). Stakeholders agreed on the most suitable biogas project areas despite their different decision-making styles and criteria scores, with no identification of level 9 suitability. Policy-makers favoured northern (Yicheng, Zhongxiang, Jingshan, and Tianmen), western (Shayang), and southeastern (Jianli) locations (Fig. S15(b)). This comparison shows experts' wide site recognition, policy-makers' strategic focus, and residents' selectivity, underscoring the importance of integrating diverse perspectives for optimal site selection that balances expertise, policy goals, and local preferences.

In general, the analysis revealed a complex suitability network across plains with central prime sites and potential areas such as 'Env-3', 'Soc-7', and 'Eco-9' on the flanks.

3.5. Network decision-making under spatio-temporal scenarios

3.5.1. Biogas plant candidates

Considering the land-use area (16,380 m² for ABPs) and a minimum distance of 0.5 km to avoid interference, a 2-ha threshold filtered out unsuitable areas (Ferrari et al., 2021b). By overlaying the biogas

potential with spatiotemporal stability, this process transformed raster data (levels 7–9) into points, generating candidate points for three stability scenarios and various decision-making perspectives. Fig. S16 reveals that the experts in Scenario I targeted a few key areas for biogas candidates, with Scenario II showing their increased openness to moderate-stability regions, and Scenario III further widening the net (49 % increase at the plain level, compared to Scenario I), especially in Yicheng (62 % increase compared to Scenario I) and Zhongxiang (146 % increase). Policy-makers started conservatively in Scenario I, focusing on Jingshan (149 candidates), Yicheng (320 candidates), and Jiangling (11 candidates), but by Scenario III, they significantly broadened their scope (24 % increase at the plain level), particularly in Jingshan (82 % increase) and Zhongxiang (from 2 candidates to 16), suggesting a balance between crop stability and socioeconomic factors. Local residents concentrated their choices in Shayang (1235 candidates) and Yicheng (821) in Scenario I. Nevertheless, by Scenario III, they showed the greatest flexibility, with considerable increases in candidates across various regions (38 % increases at the plain level), reflecting their adaptability to the evolving stability criteria.

Overall, Fig. S16(d) shows that Shayang is a preferred biogas site, with Yicheng gaining interest from experts and residents in less intense
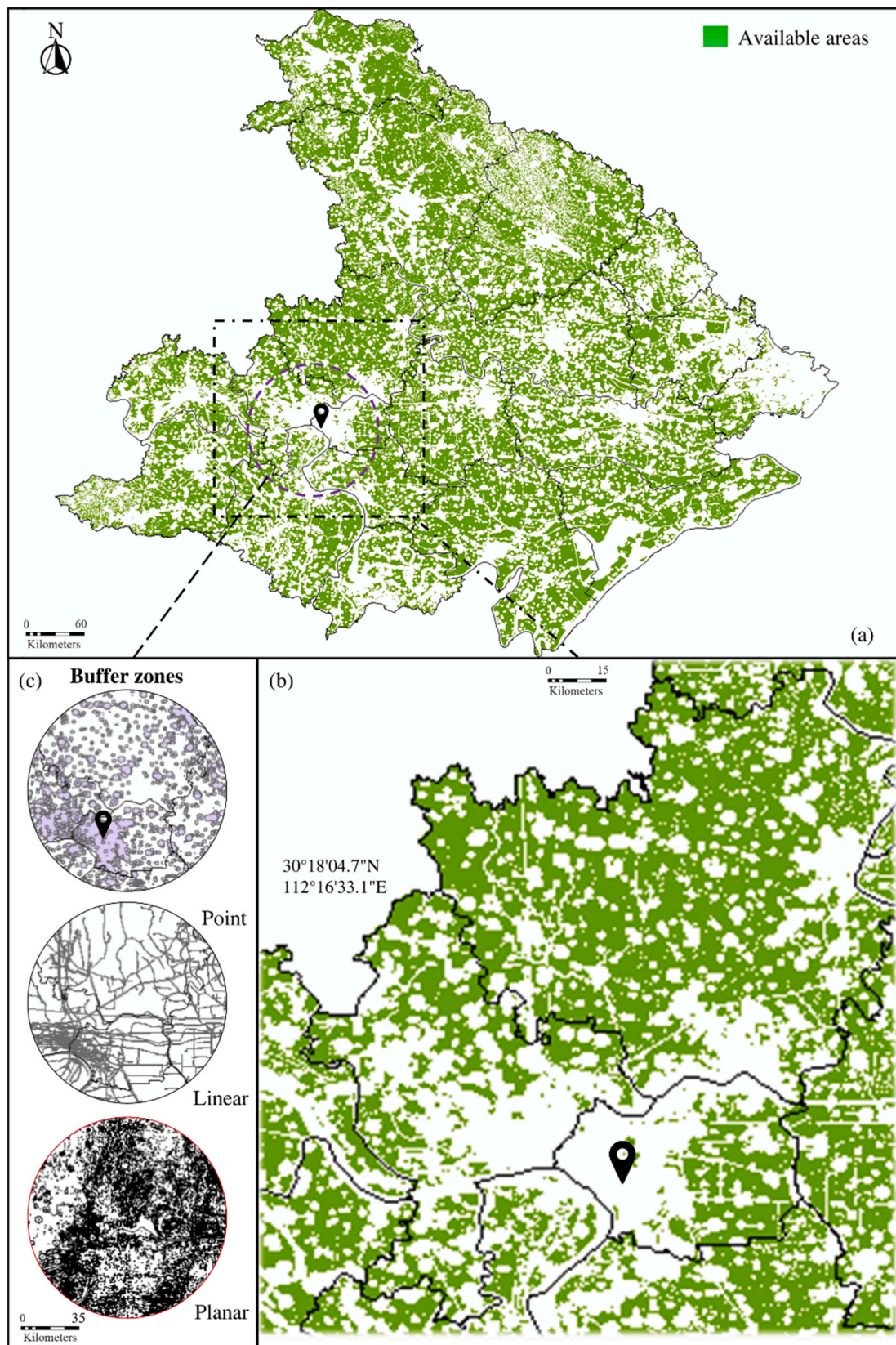
Fig. 6. Available and restricted areas for siting biogas plants: (a) available areas in the plain, (b) local magnification of available areas, (c) local restricted/buffer zones (see Figs. S8–S11 for more details).
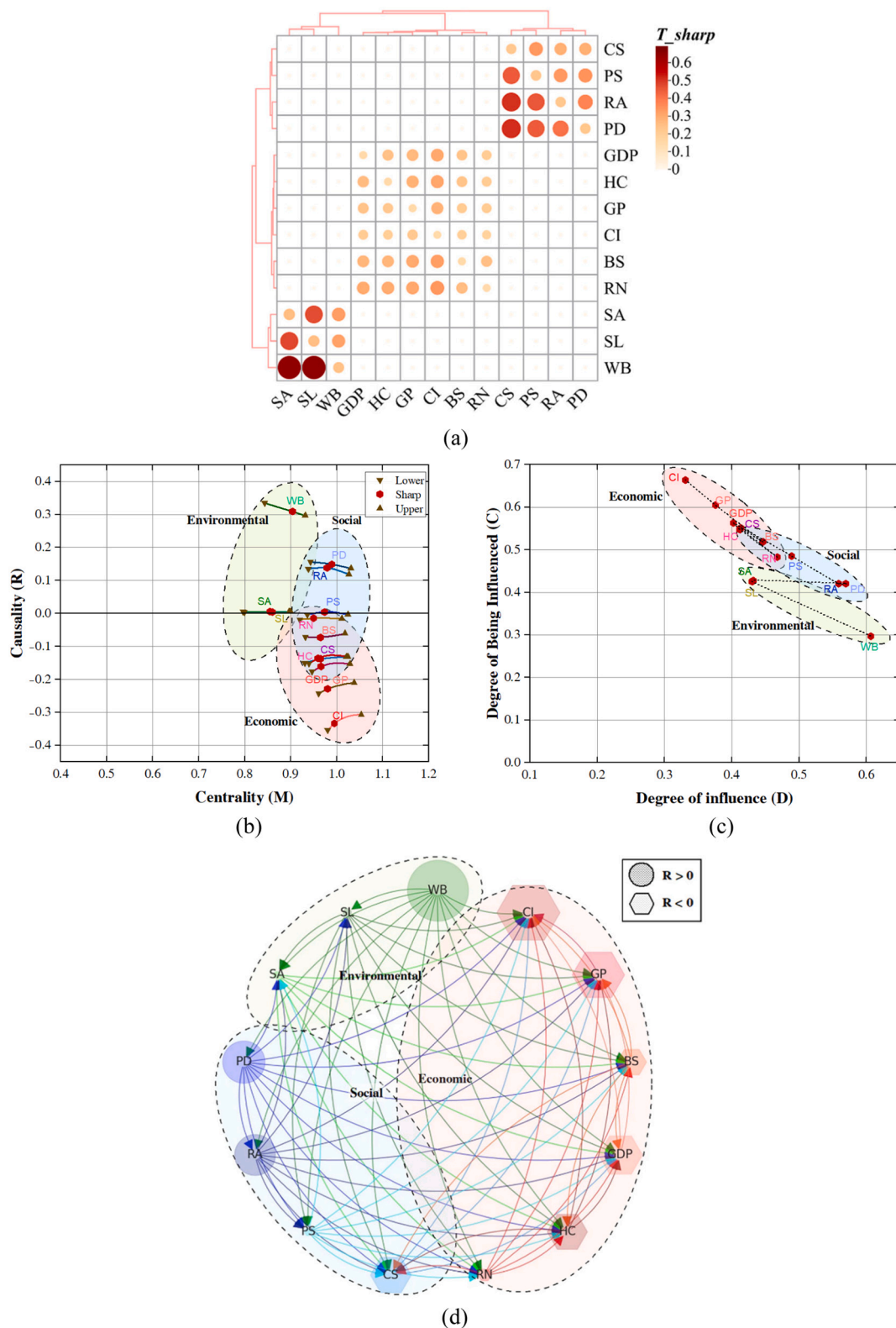
Fig. 7. MCDA decisions of experts: (a) total relation matrices (T_{sharp}) heatmap, (b) trajectory plots for centrality-causality (M-R), (c) influencing-influenced (D—C) linkage and scatterplot, and (d) causal network diagram. The heatmap used Pearson correlation and complete-linkage clustering with Euclidean distance, including a hierarchical dendrogram. The M-R and D—C graphs show the DEMATEL results via Eqs. (1)–(3), highlighting the driving forces and relationships dynamically shown in the network diagram (the shape size represents the |R| value). Fig. S12 shows the decisions of policy-makers and locals.
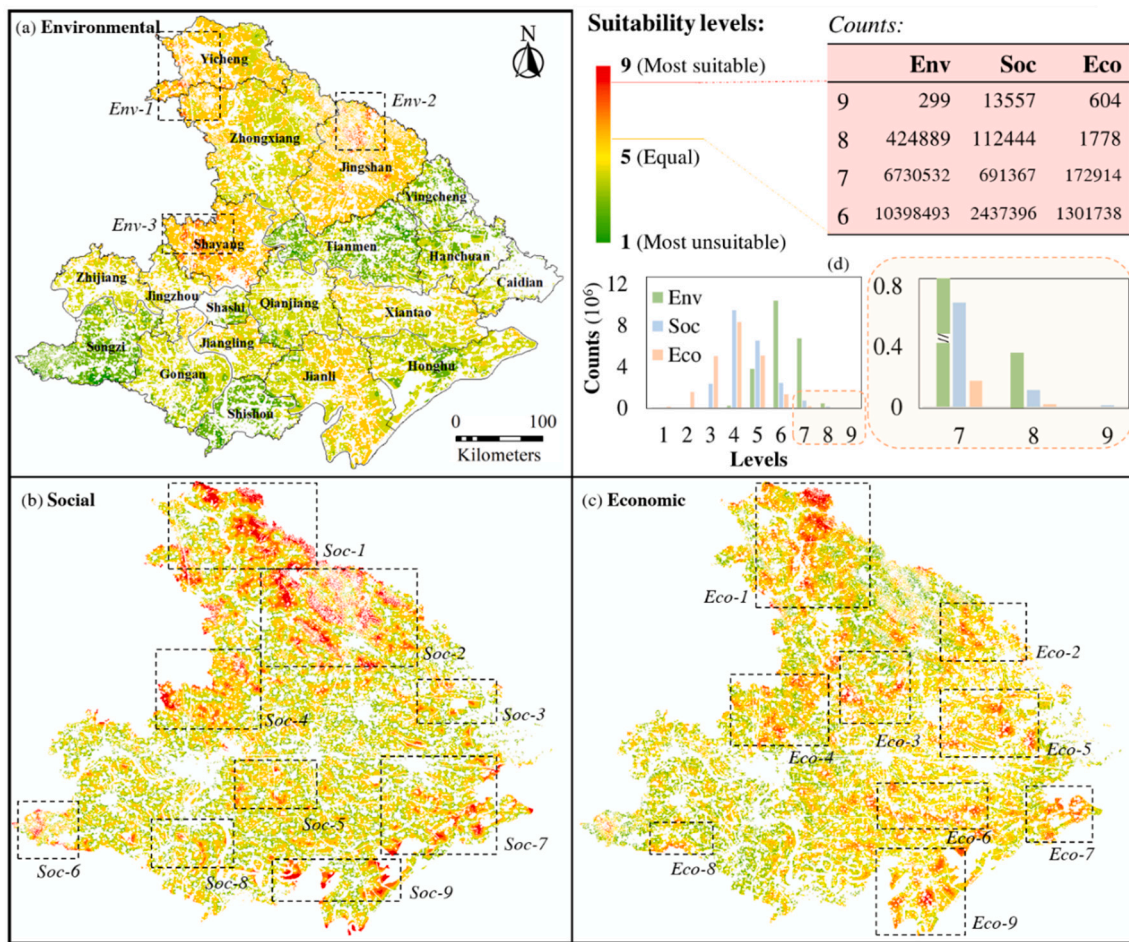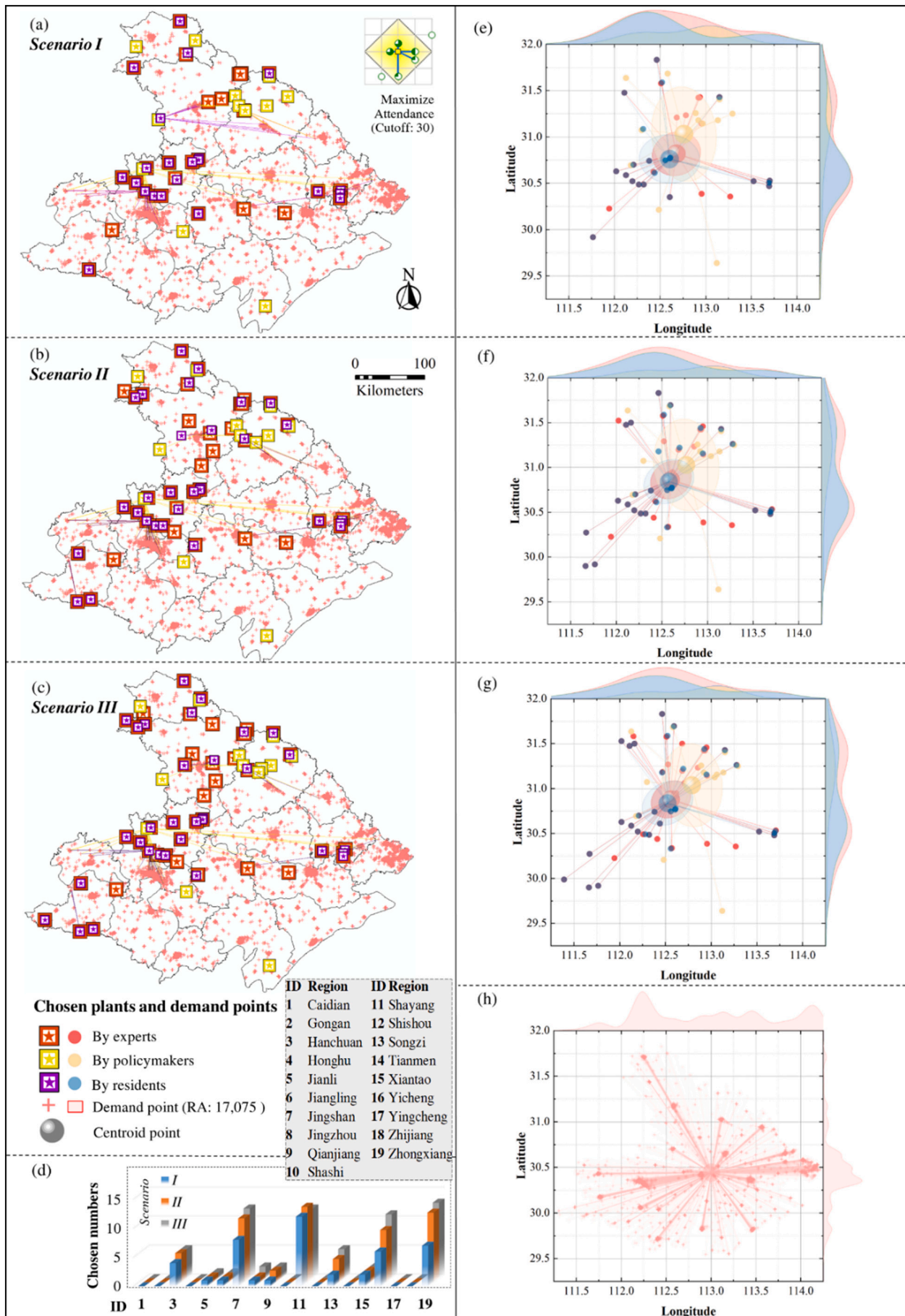
Fig. 8. Suitability maps assessed by (a) environmental (Env), (b) social (Soc), (c) economic (Eco), and (d) pixel counts with 9 suitability levels based on three criteria.

(a) Scenario I — Maximize Attendance (Cutoff: 30)

(b) Scenario II

(c) Scenario III

Chosen plants and demand points
- By experts
- By policymakers
- By residents
- Demand point (RA: 17,075)
- Centroid point

ID	Region	ID	Region
1	Caidian	11	Shayang
2	Gongan	12	Shishou
3	Hanchuan	13	Songzi
4	Honghu	14	Tianmen
5	Jianli	15	Xiantao
6	Jiangling	16	Yicheng
7	Jingshan	17	Yingcheng
8	Jingzhou	18	Zhijiang
9	Qianjiang	19	Zhongxiang
10	Shashi		

(d) Chosen numbers — Scenario I, II, III

(e), (f), (g), (h)

(caption on next page)

Fig. 9. Biogas plant sites and distribution across scenarios: (a) Scenario I plants, (b) Scenario II plants, (c) Scenario III plants, (d) zonal plant statistics, (e) Scenario I coordinates with marginal plots, (f) Scenario II coordinates, (g) Scenario III coordinates, (h) demand point distribution. The 'Location-Allocation' tool in Network Analyst modelled plant distribution using 'Maximise Attendance' with a linear cost function and a 30 km cut-off. The centroid ellipse is at 95 % confidence, and the marginal curves used kernel smoothing parameters (Table S11).

scenarios, while policy-makers favoured Jingshan, reflecting varied evaluation criteria. Caidian, Gongan, Honghu, and Shishou were excluded due to unsuitability. The candidate site expansion from Scenarios I-III indicates a shift towards more inclusive selection criteria.

3.5.2. Selected sites for biogas plant development

This study focused on large-scale biogas plants, with RA locations (17,075) serving as demand points, which were equally weighted to candidate points in Network Analyst. Fig. 9 shows 45 facilities selected in Scenario I, increasing to 61 in Scenario II and 66 in Scenario III, with experts having the most influence on site selection (decision-making share 64–65 %, Table S12). Local residents had a significant impact (33–52 %), while policy-makers contributed the least (20–27 %). The analysis indicates that expert and resident choices align with higher demand and more efficient solutions due to the weighted analysis of demand points.

For Scenarios I-III, Fig. S17 shows site selection clustering around specific coordinates but with overall dispersion, indicating spread-out facilities. In Fig. 9(a)–(c), expert and resident decisions aligned with energy supply needs to the west and south, while policy-makers focused on the east and north, highlighting geographical differences in decision-making.

Furthermore, by examining the centroid differences between various decisions and stability in Fig. 9(e)–(h), we found that the preferences of these stakeholders varied across different scenarios. The demand centroid was (30.445, 113.002). For Scenario I, the intercentroid distances ranged from 9.6 km (expert-resident) to 33.4 km (policy-resident), and their distances to the demand centroid ranged from 51.7 km (expert) to 68.8 km (policy-maker). For Scenario II, the distances ranged from 3.1 km (expert-resident) to 27.4 km (policy-resident), and the demand centroid ranged from 60.1 km (resident) to 68.4 (policy-maker). For Scenario III, distances ranged from 6 km (expert-resident) to 33.8 km (policy-resident), and the demand centroid ranged from 63.4 km (resident) to 68.8 km (policy-maker).

Accordingly, the intercentroid distances reveal varying stakeholder agreement across the stability scenarios, with Scenario II showing the closest alignment between experts and local residents, suggesting that moderate stability fosters consensus. Higher stability enhances energy demand coverage through efficient straw acquisition. Farthest from demand, policy-makers could improve rural energy planning by incorporating expert and local insights, resulting in more comprehensive policies and evaluations for biogas site selection.

Practically, our analysis compared site selection with yearly bioenergy report data, focusing on large-scale biogas projects (CSY, 2022). Local biogas production partly mirrors the energy market demand. However, as listed in Table 5, the correlation coefficient ($R_{N-G}^2 = 0.57$), indicated imbalances between existing projects and demand, with some areas having excess projects and others facing shortages, affecting economic efficiency. Our study revealed stronger correlations ($R_{L-G}^2 = 0.9$ for Scenario I, 0.89 for Scenario II, and 0.88 for Scenario III), suggesting that our selections more closely match demand and promote supply-demand balance (Valenti et al., 2018).

For policy-makers, our findings provide insights into rural energy planning. High stability improves accuracy and energy coverage, whereas moderate stability fosters consistent stakeholder decisions, enhancing policy outcomes. Key counties, e.g., Zhongxiang, Shangyang, Jingshan, and Yicheng, are vital for supplying biogas to energy-demanding cities and overall plains, e.g., Jingmen, Tianmen, Jingzhou, Xiangyang, Qianjiang, and Xiaogan, supported by transport networks. For convenience, the coordinates of the selected biogas plant sites are provided in Table S13.

4. Conclusion

Our study on the Jianghan Plain, which used GIS-MCDA to evaluate biogas plant locations based on the bioenergy potential of agricultural and livestock byproducts and stability over time, yielded significant findings. The Jianghan Plain has significant bioenergy capacity (Section 2.1.3), with an estimated bioenergy content of 6.3×10^{12} kJ over 20 years and a biogas potential of 4.7×10^{11} kJ for 2020. Spatiotemporal analysis (Section 3.1) revealed consistent biomass availability (Section 3.2) from crops such as rice in Gongan and Shayang and wheat in Jiangling, which are essential for biogas production. By incorporating environmental, social, and economic criteria, our MCDA method pinpointed optimal locations for biogas plants, and varied stakeholder preferences for criteria, e.g., water bodies, slope, population density, GDP, industry, etc., influence the decision-making process (Section 3.3). Network and scenario analyses identified 45 to 66 suitable facilities, mainly in 4 key counties, showing that moderate stability in biomass supply aligns with decision-maker consensus, while more stable areas are crucial for meeting energy demands (Section 3.5). Hence, it is vital to integrate expert and local feedback in policy-making.

The methodology and findings highlight the critical role of choosing sites with reliable biomass for biogas projects, as confirmed by our stability analysis. Our GIS-MCDA framework is versatile, catering to diverse site selection needs, making it suitable for broader bioenergy applications. Incorporating stakeholder perspectives ensures that our projects align with local needs and support, while flexible scenario planning helps people navigate agricultural and environmental uncertainties. Aligning with global sustainability and carbon neutrality goals, our framework offers a practical model for bioenergy resource exploitation, which sets a precedent for policy and planning in environmental, agricultural, and renewable sectors. This signifies a step forwards in achieving environmental sustainability and an energy-efficient future.

Furthermore, testing the framework beyond the Jianghan Plain in diverse geographical and agricultural settings will validate its adaptability and scalability. Adapting our methodology for various bioenergy resources, e.g., woody biomass or municipal waste, by adjusting the MCDA criteria and inputs can broaden its application and utility.

CRediT authorship contribution statement

Zhan Shi: Writing – original draft, Software, Methodology, Investigation, Formal analysis, Conceptualization. **Francesco Marinello:** Writing – review & editing, Visualization. **Ping Ai:** Writing – review & editing. **Andrea Pezzuolo:** Writing – original draft, Validation, Supervision, Resources, Methodology, Investigation, Funding acquisition.

Table 5
Comparison of regional facility choices with survey data and evaluation of decision-making performance.

Region		Facility			Survey data	
City	County	I	II	III	Existing large-scale biogas projects (*N*)	Annual production (G, 10^4 m^3)
	Jingzhou	1	1	2		
	Shashi	0	0	0		
	Jiangling	1	1	1		
Jingzhou	Songzi	2	4	5	34	220.7
	Gongan	0	0	0		
	Shishou	0	0	0		
	Jianli	1	1	1		
	Honghu	0	0	0		
Xiantao	Xiantao	2	2	2	5	91.2
Qianjiang	Qianjiang	1	2	2	6	120
Tianmen	Tianmen	0	0	0	9	250.5
Wuhan	Caidian	0	0	0	0	0
Xiaogan	Yingcheng	0	0	0	11	104.7
	Hanchuan	4	5	5		
	Shayang	12	13	12		
Jingmen	Zhongxiang	7	12	13	33	874.4
	Jingshan	8	11	12		
Xiangyang	Yicheng	6	9	11	9	148.4
Yichang	Zhijiang	0	0	0	1	2.8
Correlation	$R^2_{I\text{-}G}$	0.90	0.89	0.88	$R^2_{N\text{-}G} = 0.57$	

$R^2_{I\text{-}G}$: Facilities from Scenarios I-III (annual gas production); $R^2_{N\text{-}G}$: Existing large-scale biogas plants (annual gas production); G: Amount required by users/markets.

Declaration of competing interest

The authors declare that they have no known competing financial interests or personal relationships that could have appeared to influence the work reported in this paper.

Data availability

The data that has been used is confidential.

Appendix A. Supplementary data

Supplementary data to this article can be found online at https://doi.org/10.1016/j.scitotenv.2024.174665.

References

2001/81/EC, D, 2001. Directive 2001/81/EC of the European Parliament and of the Council of 23 October 2001 on national emission ceilings for certain atmospheric pollutants (National Emissions Ceiling Directive). Official JL 309, 0022–0030.

Adamu, H., Bello, U., Yuguda, A.U., Tafida, U.I., Jalam, A.M., Sabo, A., Qamar, M., 2023. Production processes, techno-economic and policy challenges of bioenergy production from fruit and vegetable wastes. Renew. Sustain. Energy Rev. 186, 113686.

Bai, C., Sarkis, J., 2013. A grey-based DEMATEL model for evaluating business process management critical success factors. Int. J. Prod. Econ. 146 (1), 281–292.

Banks, T., Fischler, W., Shenker, S.H., Susskind, L., 1997. M theory as a matrix model: a conjecture. Physical Review D 55 (8), 5112–5128.

Batel, S., Devine-Wright, P., Tangeland, T., 2013. Social acceptance of low carbon energy and associated infrastructures: a critical discussion. Energy Policy 58, 1–5.

Blasch, G., Li, Z., Taylor, J.A., 2020. Multi-temporal yield pattern analysis method for deriving yield zones in crop production systems. Precis. Agric. 21 (6), 1263–1290.

Brahma, A., Saikia, K., Hiloidhari, M., Baruah, D.C., 2016. GIS based planning of a biomethanation power plant in Assam, India. Renew. Sustain. Energy Rev. 62, 596–608.

Chiumenti, A., Pezzuolo, A., Boscaro, D., da Borso, F., 2019. Exploitation of mowed grass from green areas by means of anaerobic digestion: effects of grass conservation methods (drying and ensiling) on biogas and biomethane yield. Energies 12, 3244.

CSY, 2022. China Statistical Yearbook. National Bureau of Statistics of China, Beijing.

Dong, X., Pi, G., Ma, Z., Dong, C., 2017. The reform of the natural gas industry in the PR of China. Renew. Sustain. Energy Rev. 73, 582–593.

Dreher, A., Lang, V., Reinsberg, B., 2024. Aid effectiveness and donor motives. World Dev. 176.

Elavarasan, D., 2020. Crop yield prediction using deep reinforcement learning model for sustainable agrarian applications. IEEE Access 8, 86886–86901.

EU, 2021. Directive of the European parliament and of the council as regards the promotion of energy from renewable sources. Eur. Commission 218, 5–24.

Eurostat, 2020. https://ec.europa.eu/eurostat/databrowser/NAMQ_10_GDP/default/table.

Ferrari, G., Ai, P., Alengebawy, A., Marinello, F., Pezzuolo, A., 2021a. An assessment of nitrogen loading and biogas production from Italian livestock: a multilevel and spatial analysis. J. Clean. Prod. 317.

Ferrari, G., Ioverno, F., Sozzi, M., Marinello, F., Pezzuolo, A., 2021b. Land-use change and bioenergy production: soil consumption and characterization of anaerobic digestion plants. Energies 14 (13).

Ferrari, G., Ai, P., Marinello, F., Pezzuolo, A., 2022a. Where and how? A comprehensive review of multicriteria approaches for bioenergy plant siting. J. Clean. Prod. 346.

Ferrari, G., Marinello, F., Lemmer, A., Ranzato, C., Pezzuolo, A., 2022b. Network analysis for optimal biomethane plant location through a multidisciplinary approach. J. Clean. Prod. 378.

Hajkowicz, S., Collins, K., 2007. A review of multiple criteria analysis for water resource planning and management. Water Resour. Manag. 21 (9), 1553–1566.

Huang, Y., Dong, J., Fu, J., 2014. 1 Km Grid GDP Dataset of China (2005, 2010).

IEA, 2021. An Energy Sector Roadmap to Carbon Neutrality in China. OECD Publishing.

Jeong, J.S., Ramírez-Gómez, Á., 2018. Optimizing the location of a biomass plant with a fuzzy-DEcision-MAking Trial and Evaluation Laboratory (F-DEMATEL) and multi-criteria spatial decision assessment for renewable energy management and long-term sustainability. J. Clean. Prod. 182, 509–520.

Jesus, R.H.G.D., Barros, M.V., Salvador, R., Souza, J.T.D., Piekarski, C.M., Francisco, A.C. D., 2021. Forming clusters based on strategic partnerships and circular economy for biogas production: a GIS analysis for optimal location. Biomass Bioenergy 150.

Kumar Sharma, A., Kumar Ghodke, P., Goyal, N., Nethaji, S., Chen, W.-H., 2022. Machine learning technology in biohydrogen production from agriculture waste: recent advances and future perspectives. Bioresour. Technol. 364, 128076.

Leduc, S., Lundgren, J., Franklin, O., Dotzauer, E., 2010. Location of a biomass based methanol production plant: a dynamic problem in northern Sweden. Appl. Energy 87 (1), 68–75.

Li, D., 2022. Analysis of agricultural biomass energy use and greenhouse gas reduction evidence from China. J. Environ. Public Health 2022.

Liang, F., Shi, Z., Wei, S., Wu, L., Yan, S., 2023a. What is the appropriate content of HCO3− irrigated into tomato cultivation soil for enhancing its carbon fixation? Environmental Technology & Innovation 32, 103332.

Liang, F., Shi, Z., Wei, S., Yan, S., 2023b. Biogas slurry purification-lettuce growth nexus: Nutrients absorption and pollutants removal. Sci, Total Environ, p. 890.

Liu, T., Ferrari, G., Pezzuolo, A., Alengebawy, A., Jin, K., Yang, G., Li, Q., Ai, P., 2023. Evaluation and analysis of biogas potential from agricultural waste in Hubei Province, China. Agric. Syst. 205.

Lloyd, C.T., Chamberlain, H., Kerr, D., Yetman, G., 2019. Global spatio-temporally harmonised datasets for producing high-resolution gridded population distribution datasets. Big Earth Data 3 (2), 108–139.

Luo, Y., Zhang, Z., Chen, Y., Li, Z., Tao, F., 2020. ChinaCropPhen1km: a high-resolution crop phenological dataset for three staple crops in China during 2000-2015 based on leaf area index (LAI) products. Earth Sys. Sci. Data 12 (1), 197–214.

McEntee, P.J., Bennett, S.J., Belford, R.K., 2020. Mapping the spatial and temporal stability of production in mixed farming systems: an index that integrates crop and pasture productivity to assist in the management of variability. Precis. Agric. 21 (1), 77–106.

Pascucci, S., Carfora, M.F., Palombo, A., Pignatti, S., Casa, R., Pepe, M., Castaldi, F., 2018. A comparison between standard and functional clustering methodologies: application to agricultural fields for yield pattern assessment. Remote Sens. (Basel) 10 (4), 585.

Qiu, B., Hu, X., Chen, C., Tang, Z., Yang, P., Zhu, X., Yan, C., Jian, Z., 2022. Maps of cropping patterns in China during 2015–2021. Sci. Data 9 (1).

Running, S., Zhao, M., 2021. MODIS/Terra Net Primary Production Gap-Filled Yearly L4 Global 500m SIN Grid V061. NASA EOSDIS Land Processes DAAC.

Saaty, R.W., 1987. The analytic hierarchy process-what it is and how it is used. Mathematical Modelling 9 (3–5), 161–176.

Sarker, I.H., 2022. AI-based modeling: techniques, applications and research issues towards automation, intelligent and smart systems. SN Computer Science 3 (2), 158.

Shi, Z., Ferrari, G., Ai, P., Marinello, F., Pezzuolo, A., 2023. Artificial intelligence for biomass detection, production and energy usage in rural areas: a review of technologies and applications. Sustain Energy Technol Assess 60, 103548.

Shi, Z., Ferrari, G., Ai, P., Marinello, F., Pezzuolo, A., 2024. Bioenergy potential from agricultural by-product in 2030: an AI-based spatial analysis and climate change scenarios in a Chinese region. J. Clean. Prod. 436, 140621.

Teng, Y., Lin, P.W., Chen, X.L., Wang, J.L., 2022. An analysis of the behavioral decisions of governments, village collectives, and farmers under rural waste sorting. Environ. Impact Assess, Rev, p. 95.

UNDP, 2021. United Nations Development Programme (UNDP). A Research Handbook. Springer, International Conflict and Security Law, pp. 761–777.

Valenti, F., Porto, S.M.C., Dale, B.E., Liao, W., 2018. Spatial analysis of feedstock supply and logistics to establish regional biogas power generation: a case study in the region of Sicily. Renew. Sustain. Energy Rev. 97, 50–63.

Willett, W., Rockström, J., Loken, B., Springmann, M., Lang, T., 2019. Food in the Anthropocene: the EAT–Lancet Commission on healthy diets from sustainable food systems. Lancet 393 (10170), 447–492.

Yan, B., Yan, J., Li, Y., Qin, Y., Yang, L., 2021. Spatial distribution of biogas potential, utilization ratio and development potential of biogas from agricultural waste in China. J. Clean. Prod. 292.

Zeng, J., Ribeiro-Navarrete, S., Ning, Z., Mardani, A., 2023. The intermediary effect of intelligent Amap-related traffic efficiency on haze pollution. Transportation Research Part E: Logistics and Transportation Review 178, 103262.

Zhang, T., Bu, M.d., Geng, W., 2012. Pollution status and biogas-producing potential of livestock and poultry excrements in China. Chinese J. Ecol. 31 (5), 1241–1249.

Zhao, N., Teng, J., Chen, Y., 2018. Current situation and analysis of agricultural waste management in China. World Environment 4 (4), 44–47.

Zhao, X., Zhou, Y., Chen, W., Li, X., Li, X., Li, D., 2021. Mapping hourly population dynamics using remotely sensed and geospatial data: a case study in Beijing. China. GIScience & Remote Sensing 58 (5), 717–732.